

Approval Talk [HIG-23-005]

# “Search for rare decays of the Higgs boson into a photon and a $\rho^0$ , $\phi$ or $K^{*0}$ meson”

R. Covarelli<sup>1,2</sup> M. Pelliccioni<sup>1</sup> G. Umoret<sup>1,2</sup>  
M. D'Alfonso<sup>3</sup> G. Gomez Ceballos<sup>3</sup> C. Paus<sup>3</sup> K. Yoon<sup>3</sup>

<sup>1</sup>INFN Torino, Turin, Italy

<sup>2</sup>Università degli Studi di Torino, Turin, Italy

<sup>3</sup>Massachusetts Institute of Technology, Cambridge, U.S.

March 19, 2024

# Outline

<b>About this analysis .....</b>	<b>3</b>
<b>Introduction .....</b>	<b>4</b>
<b>Analysis Strategy .....</b>	<b>7</b>
<b>Triggers .....</b>	<b>10</b>
<b>Simulated Samples .....</b>	<b>14</b>
<b>Event Selection .....</b>	<b>17</b>
<b>Multivariate Analysis Selection .....</b>	<b>23</b>
<b>Signal &amp; Background Modeling .....</b>	<b>32</b>
<b>Systematic Uncertainties .....</b>	<b>35</b>
<b>Results .....</b>	<b>37</b>
<b>Backup Slides .....</b>	<b>49</b>
<b>References .....</b>	<b>53</b>

### HIG-23-005

#### Collaboration

- Collaboration of **MIT** and **Torino** groups, targeting different Higgs production categories.

#### Conveners

- **ARC**: Anadi Canepa (chair), Stefan Spanier, Jian Wang, Angelo Giacomo Zecchinelli
- **CCLE**: Christoph Maria Ernst Paus

#### Documentation

- Relevant links: [CADI](#), [TWiki](#), [Pre-Approval Talk](#), Unblinding Talk
- Latest ANs (two individual + one combined):  
[AN-22-004](#) (MIT, v9), [AN-22-067](#) (Torino, v10), and [AN-23-004](#) (combined, v7)

# Introduction

## Higgs coupling with light quarks ( $u, d, s$ )

- Suppressed couplings and large QCD background hamper direct searches.
- Class of decays suggested  $H \rightarrow M\gamma$ , where  $M$  is a light-quark meson.
- *In this analysis,  $M = \phi, \rho^0, K^{*0}$  are considered.*

Channel	Coupling	SM $\mathcal{BR}(H \rightarrow M\gamma)$
$H \rightarrow \phi\gamma$	$s$	$(1.68 \pm 0.08) \times 10^{-5}$ [1]
$H \rightarrow \rho^0\gamma$	$u, d$	$(2.31 \pm 0.11) \times 10^{-6}$ [1]
$H \rightarrow K^{*0}\gamma$	$d\&s$ (flavor-changing)	(Only available for $H \rightarrow d\bar{s} + \bar{d}s$ ) $1.19 \times 10^{-11}$ [2]

Table 1:  $H \rightarrow M\gamma$  channels considered in this analysis with their respective couplings and predicted branching ratios.

# Motivations

## $H \rightarrow M\gamma$

### 1. Flavor-conserving probes

- **Direct contribution.** The Higgs couples via Yukawa coupling to the quarks, one of which radiates a photon.
- **Indirect contribution.** The off-shell  $\gamma^*$  or  $Z^*$  produced in  $H \rightarrow \gamma\gamma, \gamma Z^*$  fragments into a meson.

Direct and indirect contributions interfere destructively. Due to light quark masses, direct contribution is smaller than indirect. *Direct contribution is sensitive to deviation from SM.* Branching ratios are typically  $\mathcal{O}(10^{-5}-10^{-6})$ .

- $\phi$ : s quark coupling (*diagrams above*)
- $\rho^0$ : u and d quark coupling

### 2. Flavor-changing probe

- $K^{*0}$ : flavor-changing s and d quarks via weak interaction (*diagrams below*)

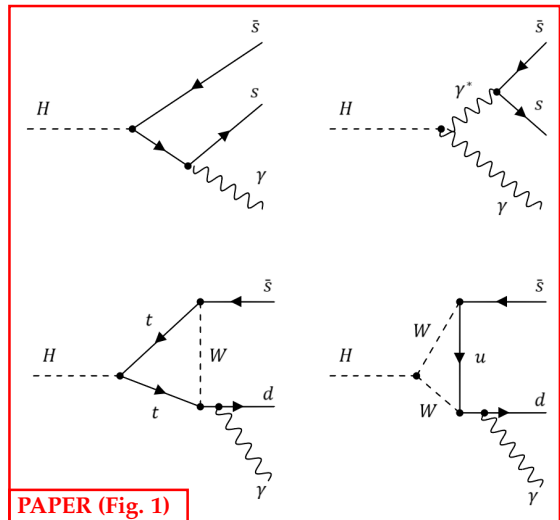


Figure 1: Feynman diagrams showing the different Higgs boson decay mechanisms into a photon and a light meson (top:  $\phi$  meson; bottom:  $K^{*0}$  meson).

# Analysis Strategy

# Analysis Strategy

- **Final states**

1. High energy **photon**.
2. High energy **di-track** from meson.



$$\mathcal{BR}(\rho^0 \rightarrow \pi^+ \pi^-) \sim 100\%$$



$$\mathcal{BR}(\phi \rightarrow K^+ K^-) \sim 49\%$$



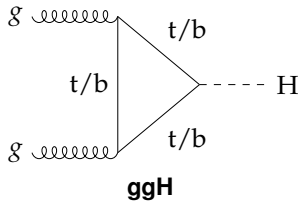
$$\mathcal{BR}(K^{*0} \rightarrow K^\pm \pi^\mp) \sim 100\%$$

Figure 2: Di-track systems for the different mesons considered in this analysis.

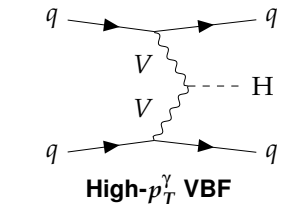
3. Signal events extracted from **photon & di-track invariant mass spectrum**.

# Analysis Strategy

- **Higgs Production Categories**



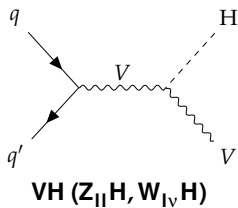
- No e/μ.



- $p_T^\gamma > 75 \text{ GeV}$ .
- No e/μ

### Low- $p_T^\gamma$ VBF

- $38 < p_T^\gamma < 75 \text{ GeV}$ .
- No e/μ



### VH ( $Z_{ll}H, W_{l\nu}H$ )

- At least one e/μ.
- Also included is  $t\bar{t}H$ , accounting for  $\sim 30\%$ .

# Triggers

# Triggers

- **High Level Triggers (HLT)**

Three types of triggers are employed.

## Tau-like trigger

### Photon + jets with $\tau$ -ID → ggH, low- $p_T^\gamma$ VBF

- Photon  $p_T^\gamma > 35$  GeV + tau-like jet  $p_T^j > 35$  GeV.
- Tau-leg similar to isolated di-track system.
- Luminosity:  
 $39.50 \text{ fb}^{-1}$  (2018).

## VBF-dedicated trigger

### High- $p_T^\gamma$ photon + VBF-like jets → high- $p_T^\gamma$ VBF

- Photon  $p_T^\gamma > 75$  GeV + di-jet with large  $M_{jj}$  and  $\Delta\eta_{jj}$ .
- Active partly during 2016-17 and fully during 2018.
- Luminosities:  
 $28.2 \text{ fb}^{-1}$  (2016),  $7.7 \text{ fb}^{-1}$  (2017),  $60 \text{ fb}^{-1}$  (2018).

## Leptonic trigger

### Double or single lepton → VH

- Single or double-muon (electron) lowest  $p_T$  thresholds vary depending on year.
- To complement selection, triggers requiring a lepton and a photon is also used.
- Luminosity:  
 $138 \text{ fb}^{-1}$  (2018).

- **HLT Efficiencies and Scale Factors**

Trigger efficiency **scale factor** defined as the ratio of data vs. MC efficiency.

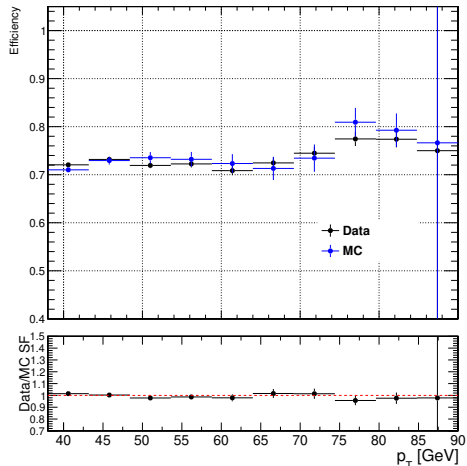
$$SF = \frac{\epsilon_{\text{Data}}}{\epsilon_{\text{MC}}}$$

- For the tau-like trigger, Data = Single Muon, MC = Drell-Yan.  
Photon-leg and tau-leg efficiencies measured separately.
- Modification on photon-leg added to reduce fake photon rate by forcing the photon to be a FSR.

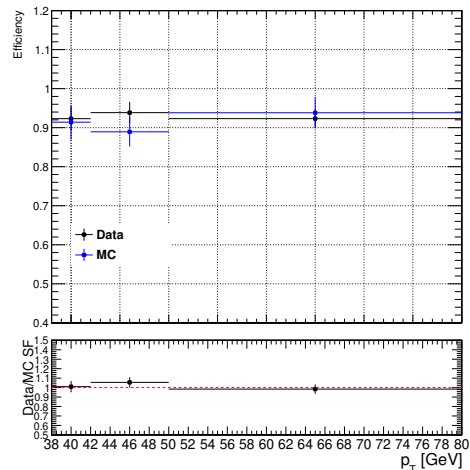
# Triggers

- **HLT Efficiencies and Scale Factors**

Tau-like trigger efficiencies MC (blue) vs. Data (black).



(a) Tau-like trigger photon-leg efficiencies for MC and data.



(b) Tau-like trigger tau-leg efficiencies for MC and data.

Figure 3: Photon-leg and tau-leg efficiencies of the tau-like trigger.

# Simulated Samples

# Simulated Samples

- **MC Generation**

Gen-level: POWHEG (NLO) or MADGRAPH5\_aMC@NLC (LO)

PDFs: NNPDF3.1 (NNLO)

Hadronization: PYTHIA 8.212

- SM processes considered in background simulation are  $\gamma$ ,  $W \rightarrow l\nu$ , Drell-Yan  $Z \rightarrow ll$  with jets,  $t\bar{t}$ ,  $W\gamma$ , and  $Z\gamma$ .
- Cross sections for Higgs production:

Process	$\sigma$ (fb)
ggH	48580
VBF	3782
$W_{l\nu}H$	471
$Z_{ll}H$	77
$ggZ_{ll}H$	12

# Simulated Samples

- **Signal Simulation**

## Polarization reweighting of events.

Higgs is a scalar, and angular momentum conservation constrains the mesons to have transverse spin alignment in the  $H \rightarrow M\gamma$  process. PYTHIA simulates unpolarized decay products. Therefore, signal events are reweighted by  $(3/2) \sin^2 \theta$ , where  $\theta$  is the angle between positive track in meson rest frame and meson flight direction in lab frame.

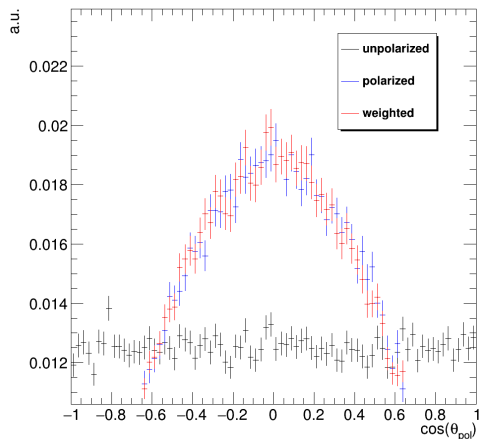


**Figure 4:**  $\cos \theta$  for the  $\rho$  meson decay. The black flat distribution illustrates the polarization angle within the centrally produced MC signal. The blue distribution portrays a privately generated MC signal wherein the accurate polarization was already incorporated. The red distribution results from reweighting the black distribution using the reweighting technique outlined in this section.

# Event Selection

# Event Selection

- **Photon selection**

	<b>ggH</b>	<b>High-<math>p_T^\gamma</math> VBF</b>	<b>Low-<math>p_T^\gamma</math> VBF</b>	<b>VH</b>
$p_T^\gamma$ [GeV]	> 38	> 75	$38 < p_T^\gamma < 75$	> 40
$ \eta^\gamma $	< 2.1	< 1.4	< 2.1	< 2.5
$\gamma$ -ID signal eff.	80%	90%	80%	90%

Table 2: Photon selection criteria across different production categories.

- $\gamma$ -ID signal eff. = MVA-based selection ID [3]
- $p_T^\gamma$  and  $|\eta^\gamma|$  cuts based on trigger thresholds and barrel vs. endcap considerations.
- ggH/VBF: conversion veto, VH: pixel veto.
- Highest- $p_T^\gamma$  photon chosen as candidate.

- **Di-track system reconstruction**

## Track selection

- Originate from PV.
- Pass “high purity” criteria.

## Meson definition

- Pair of oppositely charged tracks.
- $p_T > 5 \text{ GeV}$ ,  $|\eta| < 2.5$ .
- At least one track  $p_T > 20 \text{ GeV}$ .

## Invariant mass

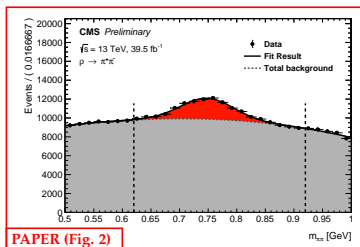
- Di-track system invariant **mass windows and sidebands** (next slide).
- $K^\pm\pi^\mp$  system: if both combinations exist, then the one closest to  $m_{K^{*0}}$  is selected.
- Reject events where  $m_{KK}$  consistent with  $m_{\pi\pi}/m_{K\pi}$  and have higher  $p_T$ , vice versa.

**Applies to all production categories.**

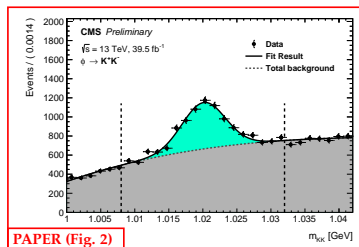
# Event Selection

- **Di-track system reconstruction**

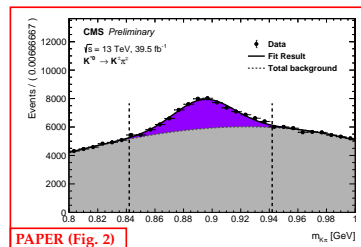
Mass windows applied to invariant mass of di-track system.



$\rho^0$  mass window:  $0.62 < m_{\pi\pi} < 0.92 \text{ GeV}$   
Sidebands:  $0.50 < m_{\pi\pi} < 0.62 \text{ GeV}$   
 $0.92 < m_{\pi\pi} < 1.00 \text{ GeV}$



$\phi$  mass window:  $1.008 < m_{KK} < 1.032 \text{ GeV}$   
Sidebands:  $1.000 < m_{KK} < 1.008 \text{ GeV}$   
 $1.032 < m_{KK} < 1.050 \text{ GeV}$



$K^{*0}$  mass window:  $0.84 < m_{K\pi} < 0.94 \text{ GeV}$   
Sidebands:  $0.80 < m_{K\pi} < 0.84 \text{ GeV}$   
 $0.94 < m_{K\pi} < 1.00 \text{ GeV}$

Figure 5: Di-track mass distribution in selected events in data, for the ggH category of the analysis,  $\rho^0 \gamma$  (left),  $\phi \gamma$  (middle) and  $K^{*0} \gamma$  (right) channels. Vertical dashed lines represent the signal mass region borders.

For more information on meson mass resolution, see backup slide 52.

# Event Selection

- **Di-track system selection**

Define the relative **charged isolation** of the leading meson candidate,

$$I^{\text{trk}}(M) = \frac{p_T^M}{p_T^M + \sum_{\text{trk}} |p_T^{\text{trk}}|},$$

and the **neutral isolation** as

$$I^{\text{neu}}(M) = \frac{p_T^M}{p_T^M + \sum_{\text{neu}} |p_T^{\text{neu}}|}.$$

$\sum_{\text{trk/neu}} |p_T^{\text{trk/neu}}|$  : sum of charged/neutral track  $p_T$  within  $\Delta R = 0.3$  of meson candidate.

	ggH	High- $p_T^\gamma$ VBF	Low- $p_T^\gamma$ VBF	VH
$p_T^M$ [GeV]	> 38	> 30	> 38	> 38
$I_M^{\text{trk}}$	> 0.9	> 0.9	> 0.9	> 0.8
$I_M^{\text{neu}}$	> 0.8	-	-	-

Table 3: Di-track system criteria across different production categories.

# Event Selection

- Event tagging

	ggH	High- $p_T^\gamma$ VBF	Low- $p_T^\gamma$ VBF	VH
Event tagging	Meson candidate within a jet with $p_T^j > 40$ GeV, tracks with $\Delta R < 0.07$	2 jets with $p_T^j > 40$ GeV, $m_{jj} > 400$ GeV, $\eta_{jj} > 3$	2 jets with $p_T^j > 30, 20$ GeV, $m_{jj} > 300$ GeV, $\eta_{jj} > 3$	1 selected and isolated $e/\mu$ or 2 selected $e/\mu$ compatible with $m_Z$

Table 4: Event tagging selection criteria across different production categories.

# Multivariate Analysis Selection

- **Multivariate Analysis (MVA) Overview**

## Motivation

Improvement of signal-to-background ratio in categories with backgrounds dominated by  $\gamma + \text{jet}$  and multijet events. → **ggH, low- $p_T^\gamma$  VBF**, and **high- $p_T^\gamma$  VBF** categories.

## Methodology

- BDT classifiers based on ROOT TMVA [4], optimized with the Gradient boosting method.
- Training and validation samples defined by **meson mass SR & sidebands**.
- Signal & Background events weighted by  $1/(\sigma M/M)$ , where

$$\frac{\sigma M}{M} = \sqrt{\left(\frac{\sigma M}{M}\right)_{\text{meson}}^2 + \left(\frac{\sigma E}{E}\right)_\gamma^2}$$

- BDT classification is further split into **two sub-categories** (“cat0” and “cat1”) based on optimized discriminator threshold values to improve upper limit results.

# Multivariate Analysis Selection

- MVA Overview

Input variables:

	ggH	High- $p_T^\gamma$ VBF	Low- $p_T^\gamma$ VBF
Kinematics	$p_T^\gamma$	$p_T^{M\gamma}$	$p_T^{M\gamma}$
	$p_T^M$	$p_T^\gamma$	$p_T^\gamma$
	$\eta_M$	$p_T^M/m_{M\gamma}$	$p_T^M/m_{M\gamma}$
Charged Isolation	$I^{\text{trk}}(\text{trk}_1)$	$I^{\text{trk}}(M)$	$I^{\text{trk}}(M)$
Photon ID		$\gamma$ mvaID	$\gamma$ mvaID
Jet-related		$M_{jj}$	$M_{jj}$
		$\Delta\phi_{jj}$	$\Delta\phi_{jj}$
		$z^*$	$z^*$

Table 5: Input variables used for ggH and VBF categories.

$z^*$  is the Zeppenfeld variable, defined as  $z^* = |\eta_{M\gamma} - 0.5(\eta_{j1} + \eta_{j2})| / |\Delta\eta_{jj}|$ .

# Multivariate Analysis Selection

- MVA: ggH category

- Training samples

**Signal:** MC-generated.

**Background:** Data from meson mass sidebands.

- 4 input variables

$p_T^\gamma$	photon $p_T$
$p_T^M$	meson $p_T$
$\eta_M$	meson $\eta$
$I^{\text{trk}}(\text{trk}_1)$	leading-track charged isolation

- BDT sub-categories

cat0: BDT-score > 0.55, optimized for max value of  $S/\sqrt{B}$ .

cat1:  $-0.4 < \text{BDT-score} < 0.55$

# Multivariate Analysis Selection

- MVA: ggH category

- Training results:

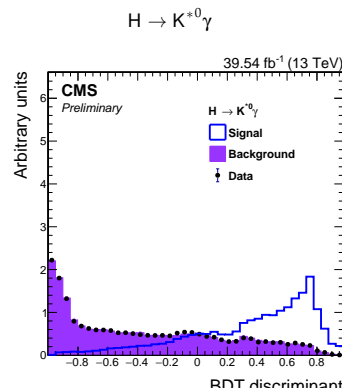
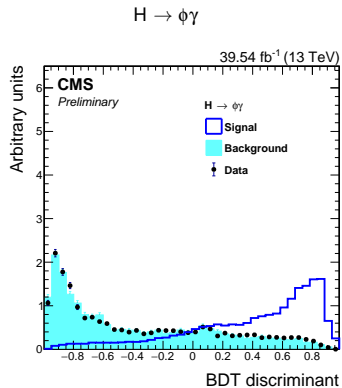
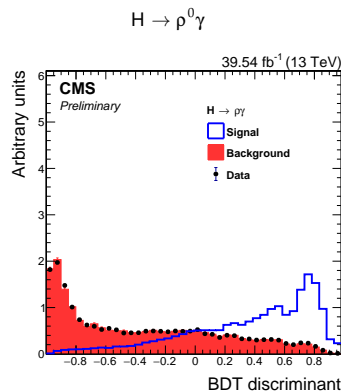


Figure 6: BDT-score shown for the three decay channels of ggH.

# Multivariate Analysis Selection

- **MVA: High & Low- $p_T^\gamma$  VBF categories**

- Training samples

**Signal:** MC-generated.

**Background:**  $\gamma$ +jets simulation and  $\gamma$  di-track events where the two tracks have the same charge.

- 8 input variables

Variable that is correlated with Higgs candidate mass is divided by the mass.

$p_T^{M\gamma}$	Higgs candidate $p_T$
$p_T^\gamma$	photon $p_T$
$p_T^M / m_{M\gamma}$	meson $p_T$ divided by Higgs candidate mass
$I^{\text{trk}}(M)$	meson charged isolation
$\gamma$ mvalID	photon identification discriminator
$M_{jj}$	di-jet invariant mass
$\Delta\phi_{jj}$	$\Delta\phi$ of the two jets
$z^*$	Zeppenfeld variable

- BDT sub-categories

cat0: BDT-score  $> 0.7$ , optimized for max value of  $S/\sqrt{B}$ .

cat1:  $-0.6 < \text{BDT-score} < 0.7$

# Multivariate Analysis Selection

- **MVA: High- $p_T^\gamma$  category**

- Training results:

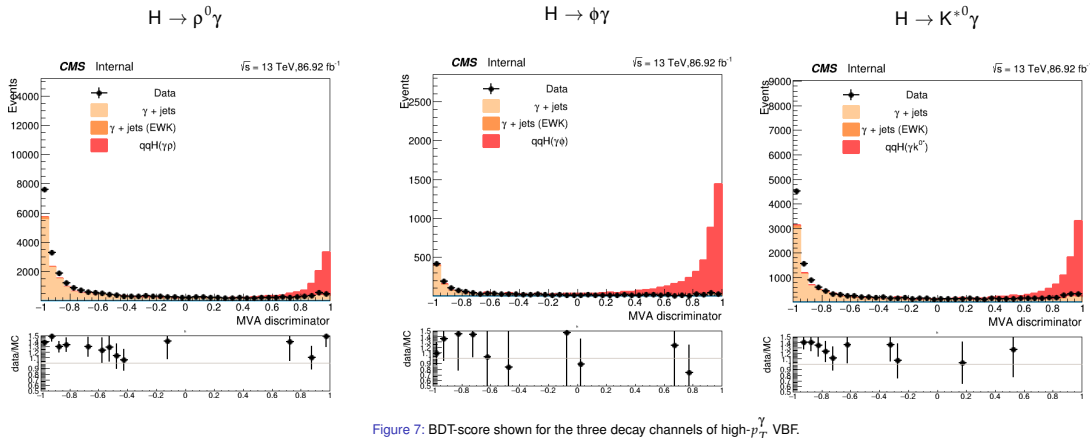


Figure 7: BDT-score shown for the three decay channels of high- $p_T^\gamma$  VBF.

# Multivariate Analysis Selection

- **MVA: Low- $p_T^\gamma$  category**

- Training results:

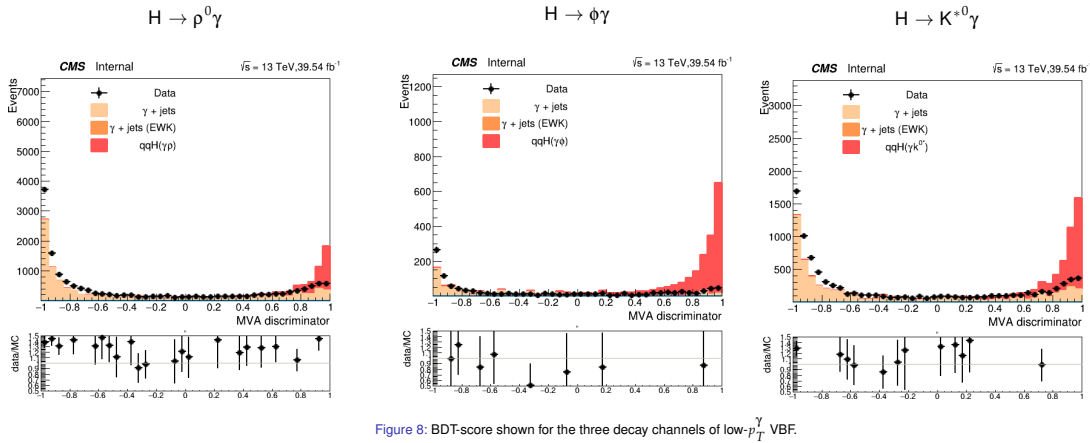


Figure 8: BDT-score shown for the three decay channels of low- $p_T^\gamma$  VBF.

# Event Selection

## Summary of Event Selection

Common selections				
2 "high-purity" tracks, opposite sign				
$ \eta^{\text{trk}}  < 2.5, p_T^{\text{trk}1} > 20 \text{ GeV}, p_T^{\text{trk}2} > 5 \text{ GeV},  \eta^M  < 2.1$				
M selection	$0.62 < m_{\pi\pi} < 0.92 \text{ GeV} (\rho^0) / 1.008 < m_{KK} < 1.032 \text{ GeV} (\phi) / 0.84 < m_{K\pi} < 0.94 \text{ GeV} (K^{*0})$			
Category	ggH	VBF high- $p_T^\gamma$	VBF low- $p_T^\gamma$	VH
Trigger	Photon + jet with $\tau$ -ID	high- $p_T$ photon + VBF-like jets	Photon + jet with $\tau$ -ID	Double or single lepton
$p_T^\gamma$ [GeV]	> 38	> 75	> 38 and < 75	> 40
$ \eta^\gamma $	< 2.5	< 1.4	< 2.1	< 2.5
$\gamma$ -ID signal eff.	80%	90%	80%	90%
$p_T^M$ [GeV]	> 38	> 30	> 38	> 38
$I^{\text{trk}}(M)$	> 0.9	> 0.9	> 0.9	> 0.8
$I^{\text{neu}}(M)$	> 0.8	-	-	-
Event tagging	Meson candidate within a jet with $p_T^j > 40$ GeV, tracks with $\Delta R < 0.07$	2 jets with $p_T^j > 40$ GeV	2 jets with $p_T^j > 30/20$ GeV	1 selected and isolated e/ $\mu$ or 2 selected e/ $\mu$ compatible with Z mass
BDT categories				
cat0	BDT > 0.55	BDT > 0.7	BDT > 0.7	-
cat1	$-0.4 < \text{BDT} < 0.55$	$-0.6 < \text{BDT} < 0.7$	$-0.6 < \text{BDT} < 0.7$	-
PAPER (Table 1)				

Figure 9: Summary of the event selections, including both common and category-specific selections.

# Signal & Background Modeling

# Signal modeling

- Signal events extracted from the distribution of the **reconstructed Higgs boson mass**.
- Analytic function: **two-tailed Crystal Ball(TTCB)**.

$$\text{TTCB}(t) = \begin{cases} e^{-t^2/2}, & \text{for } -\alpha_L < t < \alpha_R \\ (\frac{n_L}{|\alpha_L|})^{n_L} e^{-\alpha_L^2/2} (\frac{n_L}{|\alpha_L|} - |\alpha_L| - t)^{-n_L}, & \text{for } t \leq -\alpha_L \\ (\frac{n_R}{|\alpha_R|})^{n_R} e^{-\alpha_R^2/2} (\frac{n_R}{|\alpha_R|} - |\alpha_R| + t)^{-n_R}, & \text{for } t \geq \alpha_L \end{cases}$$

- Fitted via unbinned likelihood to simulated signal events.

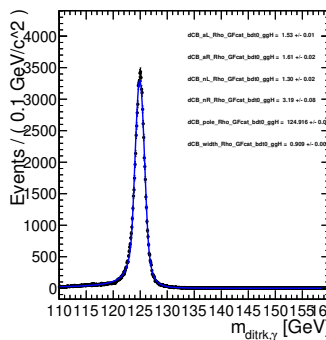


Figure 10: Example fitting of the TTCB function to the  $H \rightarrow \rho^0 \gamma$  selected signal samples from BDT cat0 in the ggH category.

- Analytic functions: **Chebychev** polynomials (main), **Bernstein** polynomials and **exponential** series (determination of shape uncertainties).
- Fitting region defined as  $m_{M\gamma}$  sidebands.
  - ggH category:  $110 < m_{M\gamma} < 120$  GeV &  $130 < m_{M\gamma} < 160$  GeV.
  - VBF categories (high & low  $p_T^\gamma$ ):  $100 < m_{M\gamma} < 120$  GeV &  $130 < m_{M\gamma} < 170$  GeV.
  - VH category:  $100 < m_{M\gamma} < 120$  GeV &  $130 < m_{M\gamma} < 150$  GeV.
- Degree of polynomial determined with **F-test**.
- **Bias studies** performed.

# Systematic Uncertainties

# Systematic Uncertainties

## Signal uncertainty

<b>Integrated Luminosity</b>	2.5% (2016), 2.3% (2017), and 2.5% (2018)
<b>Total inelastic cross section</b>	4.6%
<b>Trigger efficiencies</b>	VBF-dedicated trigger, 2.2-3.4% (photon-leg) and 5.3-5.6% (di-jet)
<b>Photon ID efficiencies</b>	Up to 1.5%, $p_T$ and $\eta$ dependent
<b>Tracking efficiency</b>	4.6% (2.3% per track)
<b>Muon/Electron ID</b>	Less than 1.0% (muons) / 1.5% (electrons)
<b>Meson Charged/Neutral Isolation Efficiencies</b>	1.7-2.8 %, depending on search channel and isolation type
<b>JEC &amp; JES</b>	Up to 3.5% in VBF, negligible in ggH
<b>QCD renormalization and factorization</b>	0.4% (VBF), 0.7% (WH), 3.8% (ZH), and 2.6% ( $t\bar{t}H$ )
<b>PDF &amp; <math>\alpha_S</math></b>	1.6-3.2%, depending on Higgs production
<b>Parton shower modeling</b>	$\mathcal{O}(0.1\%)$

Table 6: Table of systematic uncertainties.

Background shape uncertainty measured via **discrete profiling method**.

# Results

# Signal & Background Post-fit Distributions

- ggH categories

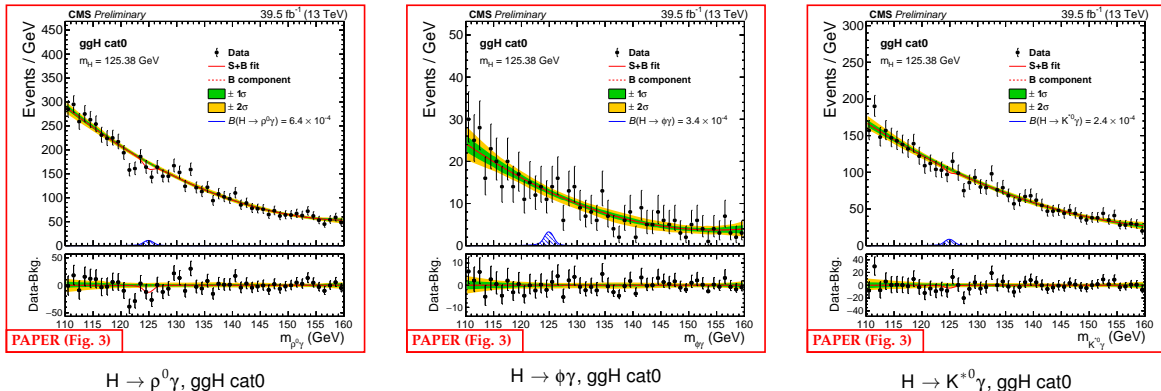
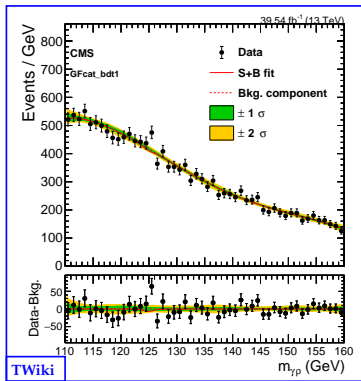


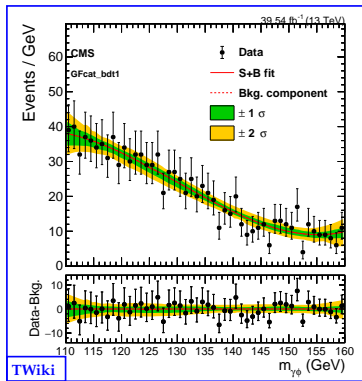
Figure 11: Post-fit  $m_{M\gamma}$  distributions in data and the background model for the ggH cat0 channels.

# Signal & Background Post-fit Distributions

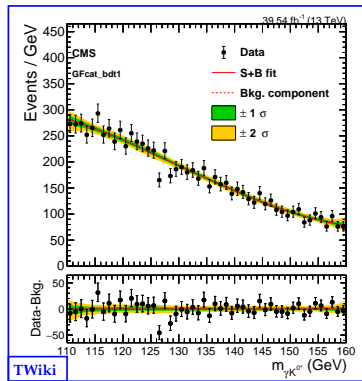
- ggH categories



$H \rightarrow \rho^0\gamma$ , ggH cat1



$H \rightarrow \phi\gamma$ , ggH cat1

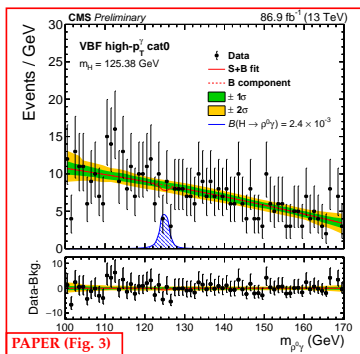


$H \rightarrow K^*\gamma$ , ggH cat1

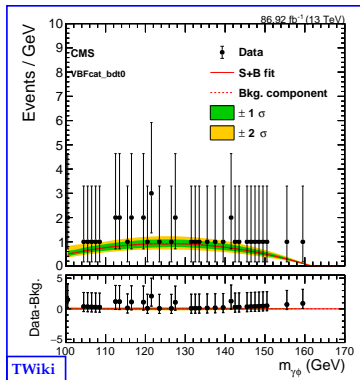
Figure 12: Post-fit  $m_{M\gamma}$  distributions in data and the background model for the ggH cat1 channels.

# Signal & Background Post-fit Distributions

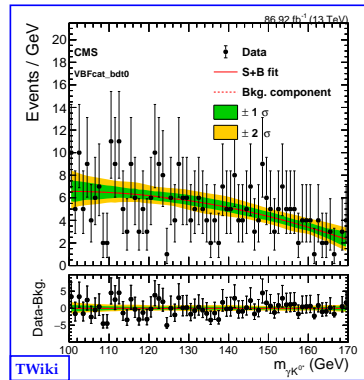
- High- $p_T^\gamma$  VBF categories



$H \rightarrow p^0\gamma$ , high- $p_T^\gamma$  VBF cat0



$H \rightarrow \phi\gamma$ , high- $p_T^\gamma$  VBF cat0

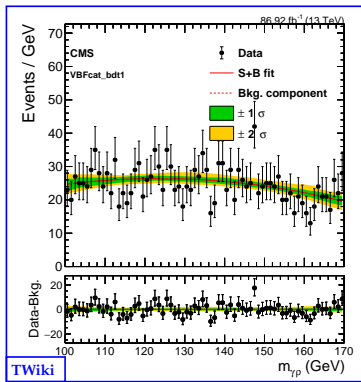


$H \rightarrow K^{*0}\gamma$ , high- $p_T^\gamma$  VBF cat0

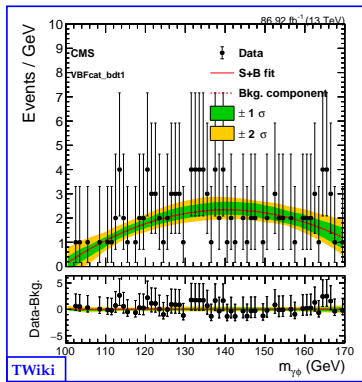
Figure 13: Post-fit  $m_{M\gamma}$  distributions in data and the background model for the high- $p_T^\gamma$  VBF cat0 channels.

# Signal & Background Post-fit Distributions

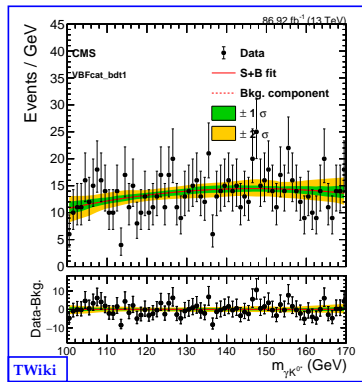
- High- $p_T^\gamma$  VBF categories



$H \rightarrow \rho^0\gamma$ , high- $p_T^\gamma$  VBF cat1



$H \rightarrow \phi\gamma$ , high- $p_T^\gamma$  VBF cat1

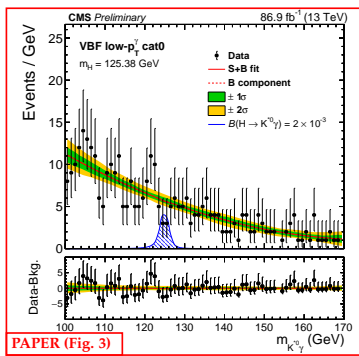


$H \rightarrow K^{*0}\gamma$ , high- $p_T^\gamma$  VBF cat1

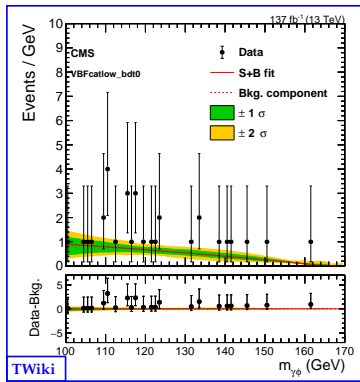
Figure 14: Post-fit  $m_{M_Y}$  distributions in data and the background model for the high- $p_T^\gamma$  cat1 channels.

# Signal & Background Post-fit Distributions

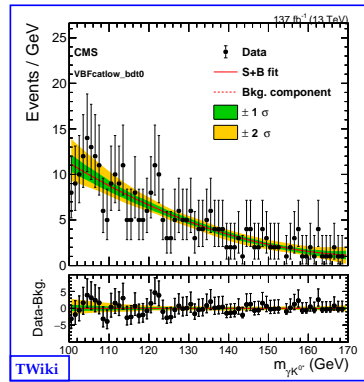
- Low- $p_T^\gamma$  VBF categories



$H \rightarrow p^0\gamma, \text{low-}p_T^\gamma \text{ VBF cat0}$



$H \rightarrow \phi\gamma, \text{low-}p_T^\gamma \text{ VBF cat0}$

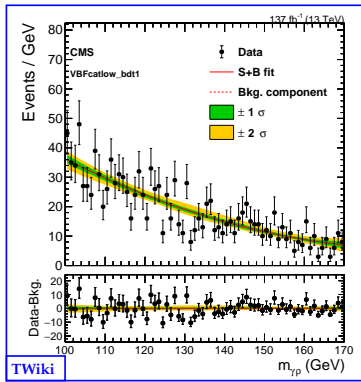


$H \rightarrow K^{*0}\gamma, \text{low-}p_T^\gamma \text{ VBF cat0}$

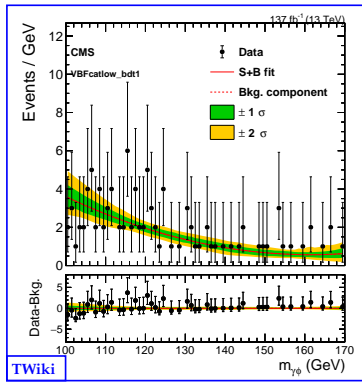
Figure 15: Post-fit  $m_{M\gamma}$  distributions in data and the background model for the low- $p_T^\gamma$  VBF cat0 channels.

# Signal & Background Post-fit Distributions

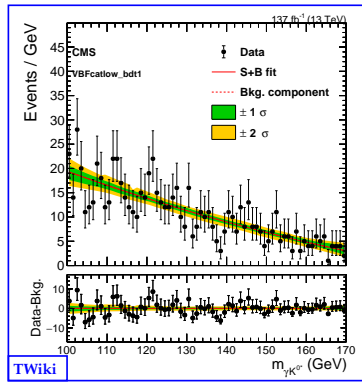
- Low- $p_T^\gamma$  VBF categories



$H \rightarrow p^0\gamma$ , low- $p_T^\gamma$  VBF cat1



$H \rightarrow \phi\gamma$ , low- $p_T^\gamma$  VBF cat1

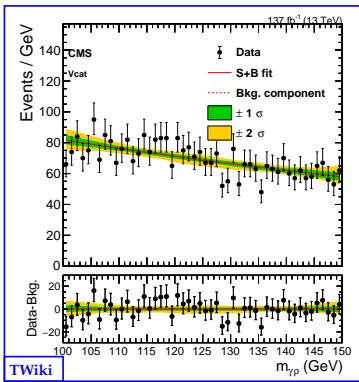


$H \rightarrow K^{*0}\gamma$ , low- $p_T^\gamma$  VBF cat1

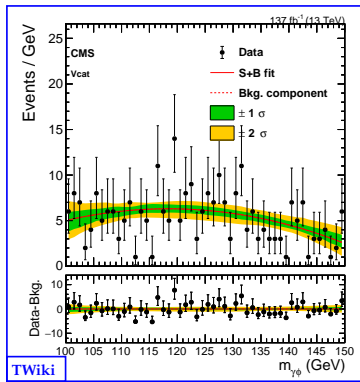
Figure 16: Post-fit  $m_{M_\gamma}$  distributions in data and the background model for the low- $p_T^\gamma$  cat1 channels.

# Signal & Background Post-fit Distributions

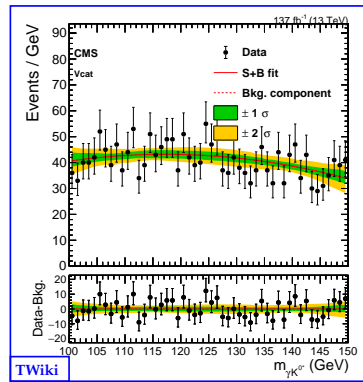
- VH categories



$H \rightarrow \rho^0 \gamma, VH$



$H \rightarrow \phi \gamma, VH$



$H \rightarrow K^{*0} \gamma, VH$

Figure 17: Post-fit  $m_{M\gamma}$  distributions in data and the background model for the VH channels.

## Upper Limits

- **Upper limits** on  $\mathcal{B}(H \rightarrow \rho^0\gamma)$ ,  $\mathcal{B}(H \rightarrow \phi\gamma)$ , and  $\mathcal{B}(H \rightarrow K^{*0}\gamma)$  set at 95% CL.
- CLs profile-likelihood ratio used as test-statistics, with the asymptotic approximation.
- Systematic uncertainties treated as nuisance parameters.

# Upper Limits

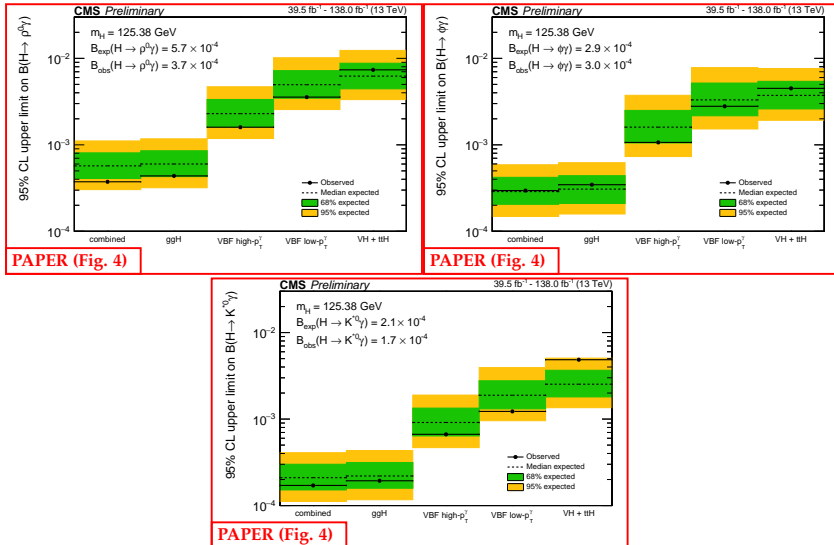


Figure 18: Expected and observed upper limits on  $B(H \rightarrow \rho^0 \gamma)$  (top left),  $B(H \rightarrow \phi \gamma)$  (top right), and  $B(H \rightarrow K_0^* \gamma)$  (bottom) split by analysis categories and combined. Green and yellow bands correspond to 1 and  $2\sigma$  confidence intervals in the expected upper limits.

## Results

	U.L. $\mathcal{B}(H \rightarrow \rho^0 \gamma)$		U.L. $\mathcal{B}(H \rightarrow \phi \gamma)$		U.L. $\mathcal{B}(H \rightarrow K^{*0} \gamma)$	
category	Exp. $(10^{-4})$	Obs. $(10^{-4})$	Exp. $(10^{-4})$	Obs. $(10^{-4})$	Exp. $(10^{-4})$	Obs. $(10^{-4})$
VH	$62.3^{+25.6}_{-17.9}$	73.7	$37.3^{+16.9}_{-11.3}$	45.0	$25.3^{+11.4}_{-7.3}$	48.5
low- $p_T^\gamma$ VBF	$49.6^{+22.5}_{-15.0}$	35.6	$33.1^{+18.7}_{-11.5}$	27.9	$18.8^{+8.90}_{-5.7}$	12.3
high- $p_T^\gamma$ VBF	$22.9^{+10.5}_{-6.9}$	16.0	$16.0^{+9.0}_{-5.5}$	10.7	$9.13^{+4.25}_{-2.75}$	6.66
ggH	$6.01^{+2.53}_{-1.72}$	4.37	$3.08^{+1.33}_{-0.98}$	3.46	$2.20^{+0.94}_{-0.62}$	1.93
combined	$5.71^{+2.37}_{-1.63}$	3.74	$2.88^{+1.33}_{-0.83}$	2.97	$2.10^{+0.90}_{-0.58}$	1.71

PAPER (Table 2)

Figure 19: Exclusion limits at 95% CL on the branching fractions of the H boson decays. Observed and median expected limits with the upper and lower bounds in the expected 68% CL intervals are reported.

## Results Comparison

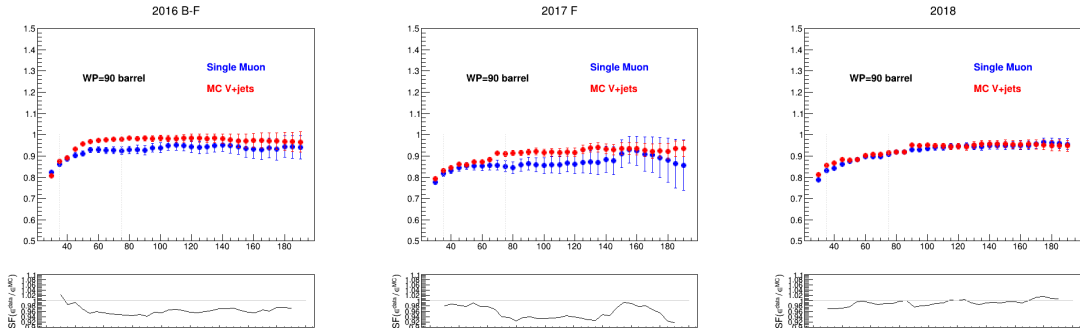
Channel	Coupling	SM $\mathcal{BR}(H \rightarrow M\gamma)$	ATLAS Limits ( $10^{-4}$ )	Our Limits ( $10^{-4}$ )
$H \rightarrow \rho^0 \gamma$	$u, d$	$(2.31 \pm 0.11) \times 10^{-6}$ [1]	Exp. $10.0^{+4.9}_{-2.8}$ Obs. $10.4$ [5]	<b>Exp. <math>5.71^{+2.37}_{-1.63}</math></b> <b>Obs. <math>3.74</math></b>
$H \rightarrow \phi \gamma$	$s$	$(1.68 \pm 0.08) \times 10^{-5}$ [1]	Exp. $4.2^{+1.8}_{-1.2}$ Obs. $5.0$ [5]	<b>Exp. <math>2.88^{+1.33}_{-0.83}</math></b> <b>Obs. <math>2.97</math></b>
$H \rightarrow K^{*0} \gamma$	$d\&s$ (flavor-changing)	(Only available for $H \rightarrow d\bar{s} + \bar{d}s$ ) $1.19 \times 10^{-11}$ [2]	Exp. $3.7^{+1.5}_{-1.0}$ Obs. $2.2$ [6]	<b>Exp. <math>2.10^{+0.90}_{-0.58}</math></b> <b>Obs. <math>1.71</math></b>

Table 7: Comparison of branching ratios obtained from theory, ATLAS, and this analysis.

# Backup Slides

# VBF Triggers

- VBF-dedicated trigger efficiencies MC (red) vs. Data (blue).



(a) VBF trigger photon-leg efficiencies for MC and data.

Figure 20: VBF-dedicated trigger photon-leg efficiencies for MC and data, shown for the  $H \rightarrow p^0 \gamma$  channel in 2016 (top-left), 2017 (top-right), and 2018 (bottom).

# Di-track Isolation Scale Factors

This slide was presented during the unblinding talk.

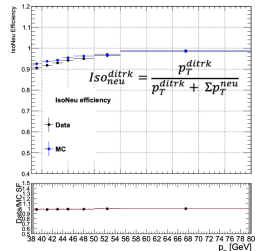
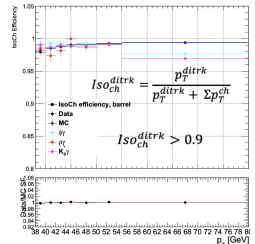
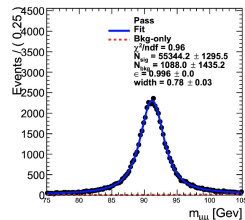
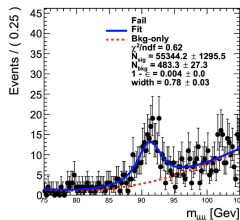


## Di-track isolation efficiency

- Strategy:  $Z \rightarrow \mu\mu$  T&P
- probe  $\mu$  used as a proxy of di-track candidate
- Efficiencies calculated for  $Iso_{ch}^{ditrk}$  and  $Iso_{neu}^{ditrk}$

### More details:

- tag  $\mu$  : must fire the IsoMu HLT, medium muonID, medium relative isolation wp
- probe  $\mu$  : no stringent requirements, no isolation requirements
- $p_T^{\mu_{probe}}$  binned scale factors
- simultaneous fit to the dimuon mass in pass and fail region
- simFit example for the last MC bin



# Meson Mass Resolution

Meson	Resolution (MeV)	Width (MeV)
$\rho^0$	90	147
$\phi$	6.4	4.25
$K^{*0}$	42	41

fig1

fig2

fig3

Figure 21: **FIX!** placeholder for figures

# References

- [1] M. König and M. Neubert, "Exclusive radiative Higgs decays as probes of light-quark Yukawa couplings", *Journal of High Energy Physics* **2015** (2015) .
- [2] J.I. Aranda, G. González-Estrada, J. Montaño et al., "Revisiting the rare  $H \rightarrow q_i q_j$  decays in the standard model", *Journal of Physics G: Nuclear and Particle Physics* **47** (2020) 125001.
- [3] CMS collaboration, "Electron and photon reconstruction and identification with the CMS experiment at the CERN LHC", *Journal of Instrumentation* **16** (2021) P05014.
- [4] A. Hoecker, P. Speckmayer, J. Stelzer et al., "TMVA - Toolkit for Multivariate Data Analysis", 2009.
- [5] ATLAS collaboration, "Erratum to: Search for exclusive Higgs and Z boson decays to  $\phi\gamma$  and  $\rho\gamma$  with the ATLAS detector", *Journal of High Energy Physics* **2023** (2023) .
- [6] ATLAS collaboration, "Search for exclusive Higgs and Z boson decays to  $\omega\gamma$  and Higgs boson decays to  $K_0^*\gamma$  with the ATLAS detector", *Physics Letters B* **847** (2023) 138292.